8712 *Biochemistry* **2009,** *48,* 8712–8720
DOI: 10.1021/bi9007758

BIOCHEMISTRY
including biophysical chemistry & molecular biology
Article

Thermodynamic Characterization of the Folding Equilibrium of the Human Nedd4-WW4 Domain: At the Frontiers of Cooperative Folding[†,‡]

Eva S. Cobos, Manuel Iglesias-Bexiga, Javier Ruiz-Sanz, Pedro L. Mateo, Irene Luque,* and Jose C. Martinez*

Department of Physical Chemistry and Institute of Biotechnology, Faculty of Sciences, University of Granada, 18071 Granada, Spain

Received May 5, 2009; Revised Manuscript Received August 6, 2009

ABSTRACT: WW domains are the smallest naturally independent β-sheet protein structures available to date and constitute attractive model systems for investigating the determinants of β-sheet folding and stability. Nonetheless, their small size and low cooperativity pose a difficult challenge for a quantitative analysis of the folding equilibrium. We describe here a comprehensive thermodynamic characterization of the conformational equilibrium of the fourth WW domain from the human ubiquitin ligase Nedd4 (hNedd4-WW4) using a combination of calorimetric and spectroscopic techniques with several denaturing agents (temperature, pH, and chemical denaturants). Our results reveal that even though the experimental data can be described in terms of a two-state equilibrium, spectral data together with anomalous values for some thermodynamic parameters (a strikingly low temperature of maximum stability, a higher than expected native-state heat capacity, and a small specific enthalpy of unfolding) could be indicative of more complex types of equilibria, such as one-state downhill folding or alternative native conformations. Moreover, double-perturbation experiments reveal some features that, in spite of the apparent linear correlation between the thermodynamic parameters, seem to be indicative of a complex conformational equilibrium in the presence of urea. In summary, the data presented here point toward the existence of a low-energy barrier between the different macrostates of hNedd4-WW4, placing it at the frontier of cooperative folding.

The analysis of model systems corresponding to isolated elements of secondary or tertiary structure has been central to the understanding of the most elementary processes that govern protein folding. Because they are amenable to simple modeling and simulation, it is possible, in combination with high-resolution experimental data, to describe the folding pathways of these simple systems at atomic resolution. This cannot be done with larger and more complex proteins, which are still inaccessible to accurate biocomputational approaches and far from current molecular dynamics time scales (*1*, *2*).

WW domains are the smallest naturally occurring β-sheet proteins identified to date. These domains adopt independent three-stranded β-sheet structures and have emerged as excellent candidates for the analysis of β-sheet folding: they are small [35−50 residues in length (Figure 1)], are highly soluble in aqueous solvents, have well-defined monomeric native states, are devoid of cofactors, prosthetic groups, disulfide bridges, and *cis*-prolines, and tolerate mutations well. Thus, they appear to be ideal model systems for tackling the experimental and computational analysis of the contribution of different forces to β-sheet folding and stability.

In spite of their interest, a relatively small number of studies have been reported for a small set of WW domains that include hYAP-WW (*2*−*6*), hPIN1-WW (*6*), and FBP28-WW (*2*, *6*−*8*). These studies have confirmed that with few exceptions WW domains are monomeric in solution and their folding transitions are reversible under most experimental conditions. In most cases, the unfolding of WW domains has been described in terms of two-state equilibrium models in spite of the fact that many of the reported results, frequently obtained exclusively by spectroscopic techniques, are not unequivocal on the matter (*2*, *3*). There is also some disagreement in the literature about the folding mechanism of small peptides similar to and/or smaller in size than WW domains for which evidence of one-state downhill folding has been reported (*9*, *10*). From an experimental point of view, downhill folders are essentially characterized by a multistate equilibrium thermal unfolding as well as by nonlinear dependencies of the thermodynamic parameters derived from a two-state analysis with denaturant agents (*11*).

It is well-established that any strategy designed to distinguish two-state from other types of equilibria should investigate protein folding using several techniques, probing different structural features, in combination with denaturant agents. In this work, we have tackled the thermodynamic characterization of the fourth WW domain from the human ubiquitin ligase Nedd4 (hNedd4-WW4)[1] combining calorimetric and spectroscopic tech-

[†]This research was financed by Grants BIO2006-15517.C02.01 from the Spanish Ministry of Education and Science and INTAS-03-51-5569 from the European Union. I.L. and E.S.C. received "Ramón y Cajal" and "Juan de la Cierva" research contracts, respectively, from the Spanish Ministry of Education and Science. We are grateful for the support of the CIC of the University of Granada.

[‡]We dedicate this paper to the memory of the late Julian M. Sturtevant for his pioneering contributions to biological microcalorimetry and biothermodynamics. Professor Mateo had the good fortune to work with him in the past and recalls with affection his example and dedication as an outstanding experimental scientist as well as his human warmth and generosity.

*To whom correspondence should be addressed. Telephone: +34 958 242370. Fax: +34 958 272879. E-mail: iluque@ugr.es (I.L.) or jcmh@ugr.es (J.C.M.).

[1]Abbreviations: Nedd4, neuronal precursor cell expressed developmentally downregulated 4; hNedd4-WW4, fourth WW domain from human ubiquitin ligase Nedd4; DSC, differential scanning calorimetry; CD, circular dichroism; N, native state; U, unfolded state; M_w, molecular weight; PDB, Protein Data Bank.

 Published on Web 08/11/2009

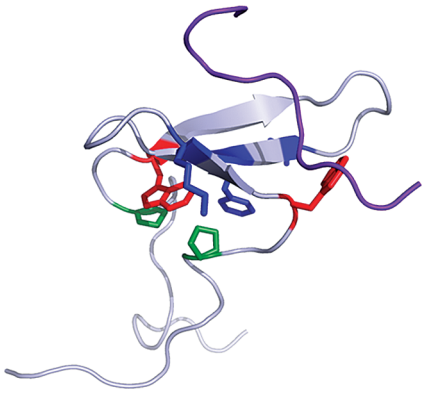

FIGURE 1: Schematic ribbon diagram of the NMR structure of the rNedd4-WW4−rENaC-βP2 peptide complex (PDB entry 1I5H). The backbone of the WW domain is represented by the gray cartoon, whereas that corresponding to the rENaC βP2 peptide is shown as a purple ribbon. Side chains of the preserved WW domain tryptophan residues are colored red, and preserved proline residues are colored green. The hydrophobic buckle established between Trp15 and Pro12 and Pro40, which has been described as being essential for maintaining the structural integrity of the WW domain (*4*), can be seen. A similar interaction is observed in the complexes involving the second invariable Trp residue (Trp37) and the proline residues from the core motif of the ligand. Residues colored blue denote differences between the rat and human WW domains. The sequence alignment of the human and rat Nedd4-WW4 domains is shown below.

niques under a wide range of conditions, including changes in temperature, pH, and denaturant concentration, which has allowed us to conduct a comprehensive multidimensional analysis of its unfolding equilibrium to reliably determine the different thermodynamic magnitudes in spite of the low cooperativity of the unfolding process. The experimental data can be reasonably described in terms of a two-state equilibrium, although anomalous values for some thermodynamic parameters, such as a strikingly low temperature of maximum stability, a higher than expected native-state heat capacity, and a small specific enthalpy of unfolding, together with some spectral features, might be comparable to those of one-state downhill folding proteins or, perhaps, could indicate some heterogeneity of the native state. Double-perturbation experiments provide further indications of the complex thermodynamic behavior of hNedd4-WW4.

EXPERIMENTAL PROCEDURES

Protein Samples. The gene encoding the hNedd4-WW4 domain was obtained by PCR using synthetic oligonucleotides as templates and extension primers. It was cloned into a pETM-30 vector (Protein Expression and Purification Core Facility, EMBL, Heidelberg, Germany) and overexpressed in *Escherichia coli* BL21/DE3 cells fused to GST and a His tag at the N-terminus. The protein was purified as described elsewhere (*12*) for similar gene constructs by means of affinity chromatography to a nickel-chelated resin (Ni-NTA agarose, QIAGEN). Samples were prepared for experimental work by extensive dialysis against a large volume (1−2 L) of the appropriate buffer, 20 mM phosphate (pH 7), 20 mM MES (pH 6), 20 mM acetate (pH 5 and 4), or 20 mM glycine (pH 3). Protein concentrations were measured by absorption at 280 nm using an extinction coefficient of 11660 cm^{-1} M^{-1}, determined as described by Gill and von Hippel (*13*), and a molecular mass of 5720 Da, as determined by mass spectrometry (Mass Spectrometry Service of the CIC, University of Granada).

Differential Scanning Calorimetry (DSC) Measurements. DSC experiments were conducted in a VP-DSC microcalorimeter (MicroCal) at a scan rate of 1.5 K/min using protein concentrations of ~1.5 mg/mL. The samples were routinely heated from 5 to 30 °C to avoid instrumental artifacts, then cooled inside the calorimeter, and heated twice from 5 to 110 °C to check the reversibility of the unfolding process. Each experimental DSC thermogram was routinely corrected from the time response of the calorimeter and from the instrumental baseline obtained with both calorimeter cells filled with the corresponding buffer. After normalization by protein concentration, the partial molar heat capacity curves [$C_{p,ap}(T)$] were calculated from the resulting thermograms assuming 0.73 mL/g for the partial specific volume and 5720 Da for the molecular mass of the hNedd4-WW4 domain. These calculations were made using ORIGIN. Thus, the baselines extracted from the analyses represent the net values for molar heat capacities and can be used as an additional criterion to justify the quality of our fitting analyses. Finally, urea samples were prepared as we will describe for CD experiments later in this section.

Differential Scanning Calorimetry (DSC) Analysis. According to the two-state model (N ⇄ U), the DSC traces were fitted individually to the following equation (see ref *14* for details):

$$C_{p,\mathrm{ap}}(T) = C_{p,\mathrm{N}} + \frac{K_{\mathrm{N-U}}}{(1 + K_{\mathrm{N-U}})^2}\frac{\Delta H_{\mathrm{N-U}}{}^2}{RT^2} + \Delta C_{p\mathrm{N-U}}\frac{K_{\mathrm{N-U}}}{1 + K_{\mathrm{N-U}}} \quad (1)$$

where $C_{p,\mathrm{ap}}(T)$ is the apparent heat capacity (in kilojoules per kelvin per mole), equivalent to the experimental DSC data, and $C_{p\mathrm{N}}$ is the heat capacity function of the native state, given by a linear function of temperature, whereas being a polynomial, the function $C_{p\mathrm{U}}$ (the heat capacity of the unfolded state) can be estimated by using the method suggested by Makhatadze and Privalov (*15*):

$$C_{p\mathrm{N}} = a + b(T - T_{\mathrm{r}}) \quad (2)$$

$$C_{p\mathrm{U}} = c + d(T - T_{\mathrm{r}}) + e(T - T_{\mathrm{r}})^2 \quad (3)$$

T_{r} is a reference temperature introduced to yield the values of the coefficients at more realistic temperatures than 0 K, which permits a direct comparison with their corresponding experimental values and avoids uncertainties deriving from unnecessarily long extrapolations. We chose a T_{r} of 293 K as a suitable value.

The temperature dependence of the equilibrium constant, according to the expression obtained from the direct integration of the van't Hoff equation, is given by

$$K_{\mathrm{N-U}} = \exp\left(\frac{\Delta S_{\mathrm{N-U}} - \frac{\Delta H_{\mathrm{N-U}}}{T}}{R}\right) \quad (4)$$

The thermodynamic functions enthalpy ($\Delta H_{\mathrm{N-U}}$), entropy ($\Delta S_{\mathrm{N-U}}$), and heat capacity ($\Delta C_{p\mathrm{N-U}}$) for the denaturation process, obtained as temperature functions according to the

Table 1: Thermodynamic Parameters of hNedd4-WW4 Domain Folding Obtained from the Global Fitting of DSC and CD Thermal Unfolding Experiments under Neutral- and Acidic-pH Conditions[a]

method	pH	T_m (°C)	ΔH_m (kJ mol^{-1})	$\Delta H_{m,exp}$ (kJ mol^{-1})	ΔC_{pN-U} (kJ K^{-1} mol^{-1})	$\Delta G_{N-U}(298)$ (kJ mol^{-1})	T_S (°C)	$\Delta G_{max}(T_S)$ (kJ mol^{-1})
CD with DSC global fitting[b]	7	58.0	133	120		11.6	−25.0	19.5
	6	46.5	100	85		5.9	−16.0	11.0
	5	37.4	73	65		2.6	−9.0	6.0
	4[c]	22.6	41			−0.3	−3.0	1.8
multiple-wavelength CD global fitting	7[c]	54.2	120		2.5	10.4		
CD thermal unfolding coupled to urea	7[c]	55.1	150		2.6	9.2		

[a]Errors have been estimated as 5% for T_m (in degrees Celsius), 10% for ΔH_m, 30% for $\Delta H_{m,exp}$, and 20% for the rest of the parameters. [b]According to the fitting procedure, together with the values of T_m and ΔH_m given, we obtained the numerical values of CD and DSC baselines, which were $\Theta_{230,N} = 15.4 - 0.04(T - 293)$; $\Theta_{230,U} = 1.21 - 0.0112(T - 293)$; $C_{pN} = 10.11 + 0.038(T - 293)$; $C_{pU} = 11.52 + \underline{0.0238}(T - 293) - \underline{0.1163 \times 10^{-3}} \times (T^2 - 293^2)$, where the underlined values were estimated from the individual contributions of amino acids and chemical groups (*15*). [c]In these cases, thermal unfolding curves were obtained via CD experiments alone.

Kirchhoff relationships, are

$$\Delta C_{pN-U} = C_{pU} - C_{pN} = A + BT + CT^2 \quad (5)$$

$$\Delta H_{N-U} = \Delta H_m + A(T - T_m) + \frac{B}{2}(T^2 - T_m{}^2) + \frac{C}{3}(T^3 - T_m{}^3) \quad (6)$$

$$\Delta S_{N-U} = \frac{\Delta S_m}{T_m} + A \ln\left(\frac{T}{T_m}\right) + B(T - T_m) + \frac{C}{2}(T^2 - T_m{}^2) \quad (7)$$

Thus, the coefficients in capital letters can be calculated from the coefficients of the C_{pN} (eq 2) and C_{pU} (eq 3) functions as

$$A = c - a - T_r(d - b) + T_r{}^2 e \quad (8)$$

$$B = d - b - (2T_r e) \quad (9)$$

$$C = e \quad (10)$$

In all the fitting strategies described in this work, we have used the values of coefficients d (0.0238 kJ K^{-2} mol^{-1}) and e (-1.163×10^{-4} kJ K^{-3} mol^{-1}) as those obtained from the polynomial function defined by the individual contributions of amino acids, allowing T_m, ΔH_m, a (the value of C_{pN} at T_r), b (the slope of C_{pN}), and c (the value of C_{pU} at T_r) to vary.

To obtain the enthalpy values as the area under the heat capacity experimental curves ($\Delta H_{m,exp}$), we have used homemade software. The N and U baselines used to calculate the excess heat capacity functions were set up according to the Takahashi and Sturtevant method (*16*). The values are listed in Table 1, where errors in these calculations should be considered to be at least 30%.

Circular Dichroism (CD) and Trp Fluorescence Measurements. CD measurements were taken in a Jasco J-715 spectropolarimeter equipped with a temperature-controlled cell holder. Far-UV CD spectra were recorded from 250 to 190 nm in a 1 mm path length cuvette using sample concentrations of 0.3 mg/mL. Near-UV CD spectra were measured from 350 to 250 nm in a 5 mm path length cuvette with sample concentrations of 1 mg/mL. Each CD spectrum was obtained by averaging 10 accumulations collected at a scan rate of 50 nm/min. All spectra were corrected by buffer contributions and then normalized as mean residue molar ellipticity.

Steady-state fluorescence measurements were taken with an Eclipse spectrofluorimeter (Cary Varian). Excitation was performed at 298 nm (5 nm slit width). Experiments were conducted in 20 mM phosphate buffer at pH 7.0 and at a protein concentration of 20 μM in a 1 cm path length cuvette.

Temperature scans were conducted at a heating rate of 1 °C/min after equilibration of the measuring cell within the cell holder at 2 °C for 10 min. When the final temperature of 98 °C was reached, the samples were incubated for 10 min to record the spectrum of the unfolded state and then cooled to 2 °C, at which point another spectrum was taken to check the reversibility of unfolding.

Stock denaturant solutions (10 M urea in water) were prepared gravimetrically in volumetric flasks, and their molar concentrations were checked by measuring the refractometry index of the solutions at 20 °C (*17*). Urea solutions were deionized using AG501-X8 ionic exchange resin (Bio-Rad). For each data point in the double-perturbation experiments, 85 μL of the dialyzed protein (1.8 mg/mL) was mixed with 415 μL of a buffered denaturant solution prepared from the stock solution. The mixtures were left to equilibrate overnight before CD thermal unfolding and spectral analysis. The usual protein concentrations in these experiments were therefore 50 μM.

Thermal Unfolding Followed by Spectroscopy and Double-Perturbation Analysis. According to the two-state model (N $\rightleftarrows$ U), thermal denaturation experiments followed by CD obtained at different urea concentrations were fitted individually to the following equation (see ref *17* for details):

$$\Theta_{235}(T) = \frac{\Theta_{235,N} + (K_{N-U}\Theta_{235,U})}{1 + K_{N-U}} \quad (11)$$

where K_{N-U} is the equilibrium constant (eq 4) and $\Theta_{230,N}$ and $\Theta_{230,U}$ correspond to the baselines for the native and unfolded states, respectively, which have been approximated by the linear functions

$$\Theta_{235,N} = f + gT \quad (12)$$

$$\Theta_{235,U} = h + iT \quad (13)$$

The thermodynamic enthalpy (ΔH_{N-U}) and entropy (ΔS_{N-U}) functions for the denaturation process are

$$\Delta H_{N-U} = \Delta H_m + \Delta C_{pN-U}(T - T_m) \quad (14)$$

$$\Delta S_{N-U} = \Delta S_m + \Delta C_{pN-U} \ln\left(\frac{T}{T_m}\right) \quad (15)$$

where the entropy change upon denaturation at T_m is $\Delta S_m = \Delta H_m/T_m$ and the heat capacity change upon denaturation (ΔC_{pN-U}) was taken to be independent of temperature.

Individual fittings of the experimental traces to the two-state model, as described by eq 11, were performed taking T_m (the denaturation temperature, where the N and U populations are equal to 50%), ΔH_m (the denaturation enthalpy value, referenced at T_m), f (the value of $\Theta_{230,N}$ at T_r), g (the slope of $\Theta_{230,N}$), h (the value of $\Theta_{230,U}$ at T_r), and i (the slope of $\Theta_{230,U}$) to be floating parameters. In the initial stages of the analysis, ΔC_{pN-U} was taken to be zero.

In the double-perturbation fittings, the optimized values for this parameter were obtained by an iterative process. In the first step, the thermal unfolding profiles at each urea concentration were individually analyzed according to a two-state equilibrium model, taking ΔC_{pN-U} to be zero. Although fitting results in this first round did not properly reproduce the experimental decay at low temperatures, the slope of the linear dependence for ΔH_m versus T_m resulted in values providing a closer estimation for the unfolding heat capacity value. This procedure was repeated until no changes in the unfolding heat capacity were obtained between two successive iterations. A parallel improvement in the normalization parameter was obtained, indicating the convergence of fitting sessions. Proceeding in this way, we arrived at an independently optimized value for ΔC_{pN-U} of 2.6 ± 0.2 kJ K^{-1} mol^{-1}.

CD−DSC Global Analysis. In our global analysis, we have considered the same heat capacity functions for the N and U states at all pH conditions, which is normal for a two-state analysis (*14*), although we calculated individually the T_m and ΔH_m values for each pH value. Thus, the CD−DSC global analysis only integrates the baselines corresponding to the N and U states. Mathematically, we used eqs 1 and 11 using the same $C_{pN}(T)$ and $C_{pU}(T)$ functions (eqs 2 and 3) for all traces. With eq 5, we can determine the ΔC_{pN-U} value of both CD and DSC experiments. Thus, the global fitting routine had 10 parameters, corresponding to the T_m and ΔH_m pair for each of the five pH conditions (ranging from 3 to 7), plus three parameters, the values of a, b, and c, which define the $C_{pN}(T)$ and $C_{pU}(T)$ functions [d and e were taken to be the values derived from Mackhatadze and Privalov's calculations (eqs 2 and 3)], and, lastly, four parameters describing both CD baselines (eqs 12 and 13). All fittings and calculations done in this work were performed by using Sigma Plot 2000 (Systat Software Inc.).

RESULTS AND DISCUSSION

hNedd4-WW4 Is Characterized by a β-II Type Far-UV CD Spectrum and Unfolds in a Single Transition. As the first step, we measured the far-UV CD spectrum of native hNedd4-WW4 (Figure 2), which is characterized by a small positive peak centered at 230 nm and an intensely negative peak at 203 nm, as reported for other WW domains (*2*−*4*). It has been proposed elsewhere (*18* and references cited therein) that the positive CD band in the 220−230 nm region is due to local interactions

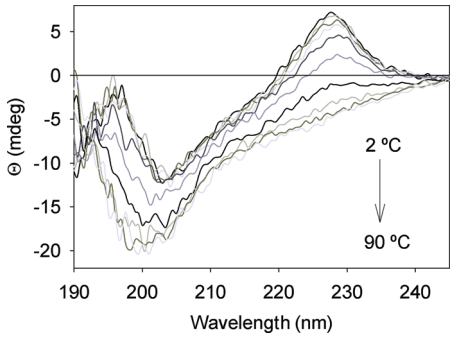

FIGURE 2: Temperature dependency of the far-UV CD spectra of hNedd4-WW4 in 20 mM phosphate buffer at pH 7. Ten far-UV spectra from 2 to 90 °C were recorded at increasing intervals of 10 °C (from top to bottom). The protein concentration was 30 μM.

involving aromatic side chains, mainly those of Trp residues in a hydrophobic microenvironment, which, in our case, is probably associated with the stacking of Trp15 with the side chains of Pro12 and Pro40 (Figure 1).

The low-wavelength region of the Nedd4-WW4 spectrum is similar to that previously reported for other β-sheet proteins containing distorted β-sheets or very short and irregular strands that resemble those of random-coil conformations (negative band around 200 nm and positive band around 185−190 nm). Proteins showing this characteristic CD behavior have been classified as β-II proteins and have a lower β-sheet/random-coil ratio than normal all-β proteins (β-I class) characterized by typical β-sheet CD spectra (negative band at 217 nm and positive peak at 195 nm) (*19*). Two main criteria have been proposed to distinguish between β-II and unfolded conformations (*20*): (i) the presence of absorption bands in the near-UV region and (ii) a sigmoidal dependence of the ellipticity signal at 203 nm upon temperature, similar to that observed at 230 nm. In this regard, our CD results clearly indicate that hNedd4-WW4 meets the criteria to be classed as a β-II protein because it shows sigmoidal thermal denaturation profiles at 203 and 260 nm, in the far- and near-UV regions, respectively (Figure 3).

Figure 3 shows the thermal denaturation profiles followed by Trp fluorescence and circular dichroism at three wavelengths (203, 230, and 260 nm) in 20 mM phosphate buffer (pH 7). The best fittings to a two-state equilibrium model obtained from a global analysis, taking a common value for the T_m and ΔH_m thermodynamic parameters, are also given (Table 1). The different baselines corresponding to the CD and/or fluorescence signals for the native and unfolded states were obtained from the analysis as independent straight lines (Figure 3). It can be seen that the experimental data can be satisfactorily described by a two-state model, providing a common set of thermodynamic parameters for the four thermal denaturation profiles as well as almost parallel baselines that show small and similar temperature dependences, as might be expected for a two-state equilibrium (*5*, *14*, *21*−*23*).

It is interesting to point out that even though a two-state equilibrium is generally associated with the existence of an isosbestic point, the hNedd4-WW4 CD spectra obtained at different temperatures do not exhibit a well-defined isodichroic point, although the different spectra tend to intersect around 195 nm. In any case, the absence of an isodichroic point has been previously described for other two-state proteins with similar β-II spectra, such as SH3 domains (*24*) or cold-shock proteins (*22*).

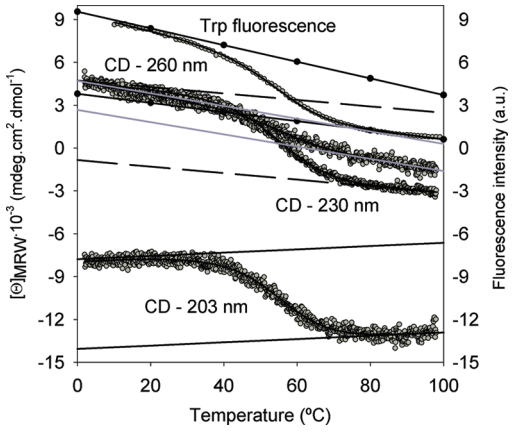

FIGURE 3: CD and Trp fluorescence thermal denaturation profiles of hNedd4-WW4 followed at different wavelengths in 20 mM phosphate buffer at pH 7 (symbols). Sample concentrations and wavelengths were 220 μM at 260 nm, 50 μM at 230 and 203 nm, and 20 μM in the fluorescence experiment. The lines through experimental data correspond to the best multiple fitting of the data to the two-state equilibrium model (eq 11) sharing ΔH_m and T_m values. The straight lines represent the baselines obtained from the fitting procedure for the native and denatured states of each thermal denaturation profile: the solid lines for 203 nm, the solid line with circles for fluorescence, the dashed line for 230 nm, and the solid gray line for 260 nm.

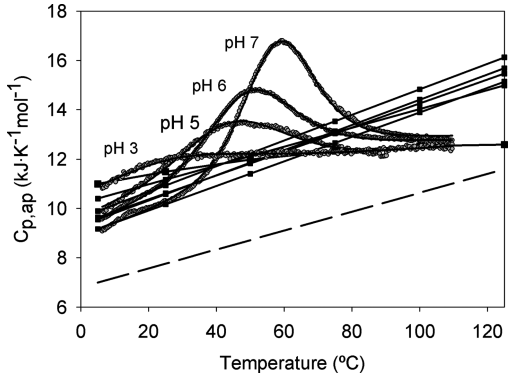

FIGURE 4: Temperature dependencies of the partial molar heat capacity, $C_{p,ap}$, of the hNedd4-WW4 domain. Empty circles correspond (from right to left) to 20 mM phosphate (pH 7), 20 mM MES (pH 6), 20 mM acetate (pH 5), and 20 mM glycine (pH 3). Solid black lines are the individual fittings for each curve to the two-state model, as described in the text. The lines with squares (■) show the heat capacities of the folded state, $C_{p,N}(T)$, and unfolded state, $C_{p,U}(T)$, obtained from the individual analyses. The dashed line represents the $C_{p,N}(T)$ function calculated according to the molecular weight (*37*).

Equilibrium Unfolding of hNedd4-WW4 Studied by CD and DSC Thermal Denaturation Profiles at Different pH Values. We studied the thermal unfolding of the hNedd4-WW4 domain by DSC and CD over the pH range from 7 to 3 (Figures 4 and 5). At low ionic strengths, in acidic and neutral solutions, the thermal unfolding of the hNedd4-WW4 domain was highly reversible (always more than 80%) and no appreciable scan rate or concentration effects could be seen for the DSC and CD traces (data not shown). Thus, the domain may be considered as being a monomeric protein that unfolds in equilibrium under these experimental conditions, a conclusion that was further confirmed by dynamic light scattering experiments, performed as described elsewhere (*12*).

We conducted a global fitting of the DSC and CD thermal unfolding curves to the two-state model. We assumed that the DSC traces obtained at the various pH values shared common $C_{pN}(T)$ and $C_{pU}(T)$ functions and the CD traces had the same N- and U-state baselines, as has been observed for typical two-state proteins such as SH3 domains (*14*). As illustrated in Figure 5, this analysis provides a reasonable description of the experimental data, with R and R_{sqr} values of 0.99. The $C_{pU}(T)$ function estimated from the tabulated contributions of individual amino acids (*15*) coincides with the experimental heat capacity data after the main transition, which has been described for other small proteins (*12*, *14*, *25*). Only a few minor deviations can be seen at high temperatures for DSC traces at pH 6 and 7, which can be ascribed to postdenaturation aggregation processes and might also be responsible for the small decrease in reversibility at these pH values (*26*).

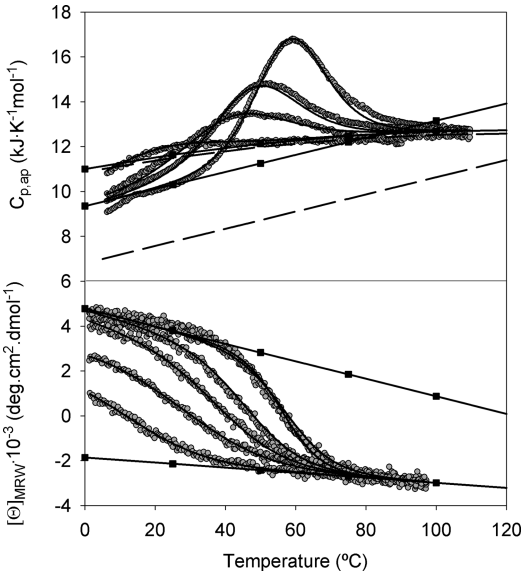

FIGURE 5: DSC and CD thermal unfolding curves of the hNedd4-WW4 domain followed at 230 nm under neutral- and acidic-pH conditions. Experimental data are represented as empty circles at different pH values (7, 6, 5, 4, and 3 from right to left). The thermal unfolding curve at pH 4 was obtained only by CD experiments. The solid lines correspond to the simultaneous global fitting to the two-state model, accepting a common temperature function of $\Delta C_{p,N-U}$ for both the DSC and CD data sets, which can be directly estimated from an analysis of the DSC experimental traces. The solid black lines with squares (■) represent the baselines for the native and denatured states obtained from the global fitting. The dashed lines represent the $C_{p,N}(T)$ function calculated according to the molecular weight (*37*) and the $C_{p,U}(T)$ function estimated from the empirical algorithm developed by Privalov and Makhatadze (*15*), based on the amino acid composition.

It is important to point out that the common $C_{pN}(T)$ and $C_{pU}(T)$ functions obtained from the global analysis intersect at 100 °C, a long way from the value of 140 °C traditionally considered to be the universal convergence temperature for representative globular proteins, but relatively close to the revised and more realistic value of 120 °C proposed recently by Privalov and co-workers (*27*). In any case, the value obtained from the global analysis is more realistic than the one obtained from the fitting of the individual DSC traces, which resulted in baselines that crossed close to the T_m (Figure 4). The global analysis also yields quite reasonable CD baselines that do not intersect within the experimental temperature range and are similar to those obtained for other small β-sheet proteins, such as SH3 domains or cold-shock proteins (*14*, *22*, *24*) and other small globular proteins (*17*, *21*, *23*).

Analysis of the baseline behavior constitutes an important matter since incorrect baselines could mask evidence for

populated intermediates and other heat contributions that might be present during the unfolding process (*16*). The robustness of the global analysis is stressed by the fact that, despite the low cooperativity of the unfolding process, all the fittings give rise to comparable results for the thermodynamic parameters whatever the baseline assumptions. Actually, the enthalpy values estimated directly from the areas of heat capacity curves ($\Delta H_{m,exp}$) are comparable with those derived from the two-state analysis despite the high errors associated with the former ones (Table 1). This is further supported by a van't Hoff to calorimetric enthalpy ratio of 0.9. Furthermore, the analysis of the data using more complex models [three-state equilibrium (*28*)] essentially reproduces the two-state fittings with no significantly populated intermediates being revealed by the deconvolution analysis (data not shown).

In summary, the equilibrium unfolding of hNedd4-WW4 can be reasonably described according to a two-state equilibrium model. It is important to note that the model accounts for the dispersion of the $C_{pN}(T)$ values at low temperatures. The close agreement between the spectroscopic and calorimetric unfolding probes is reflected in the combined analysis shown in Figures 3 and 5, although it is true that the resulting T_m values at pH 7 from the different fitting sessions exhibit a dispersion of 4 °C (Table 1), which, to a good extent, might reflect the high error in the estimation of the parameters. Nonetheless, it is interesting to note that similar discrepancies have been reported for some downhill proteins, for which experimental errors might be comparable to those shown here (*9*, *10*). In this way, the intersection of the $C_{pN}(T)$ and $C_{pU}(T)$ baselines resulting from the individual analyses at temperatures close to the T_m, which also occurs in our case (Figure 4), giving rise to a change in the sign of the unfolding heat capacity increment at unrealistic temperatures, has also been described to be indicative of downhill folding (*9*, *10*).

hNedd4-WW4 Is Characterized by a Lower Than Average Specific Enthalpy Value. In general, the normalized thermodynamic parameters provided by the two-state analysis are within the range typically observed for most small globular proteins. In fact, $\Delta H_{N-U}(330) = 3.1 \pm 0.4$ kJ (mol of residues)$^{-1}$, $\Delta S_{N-U}(330) = 9.5 \pm 1.5$ J K^{-1} (mol of residues)$^{-1}$, and $\Delta C_{p,N-U} = 50 \pm 6$ J K^{-1} (mol of residues)$^{-1}$, which coincide within a 7−15% error with those obtained for other two-state folders (*29*).

Specific enthalpy functions [$\Delta h(T) = \Delta H(T)/M_w$] typically converge at 110 °C to an average value of 54 J/g, which can be obtained by linear extrapolation of the unfolding enthalpy using the heat capacity change deriving from the linear regression of the ΔH_m versus T_m values under different pH conditions (*25*, *30*). Using 2.5 ± 0.5 kJ K^{-1} mol^{-1} for the heat capacity change as derived from the ΔH_m versus T_m regression of data from Table 1 ($r = 0.995$), we obtained a value of 45 J/g at 110 °C for the unfolding specific enthalpy of hNedd4-WW4, which is lower than the average value. Nevertheless, it is important to bear in mind that errors in these estimations, arising from the linear approximation of heat capacity functions and the long extrapolation from the temperature range of the unfolding transitions (from 20−60 to 110 °C), can be greater than 20%, especially for small proteins of low cooperativity such as hNedd4-WW4.

The convergence behavior of globular proteins has traditionally been ascribed to the fact that the hydrophobic contributions to enthalpy and entropy approach zero at the convergence temperature, so at this temperature, the unfolding enthalpy reflects mostly polar and van der Waals interactions (*30*). In this context, the fact that most globular proteins have similar specific enthalpies at the convergence temperature indicates a considerable degree of homogeneity in terms of the density and quality of the enthalpic contributions per residue (*31*). Therefore, it is reasonable to assume that the lower than average specific enthalpy obtained for hNedd-WW4 probably reflects the low cooperativity of this domain.

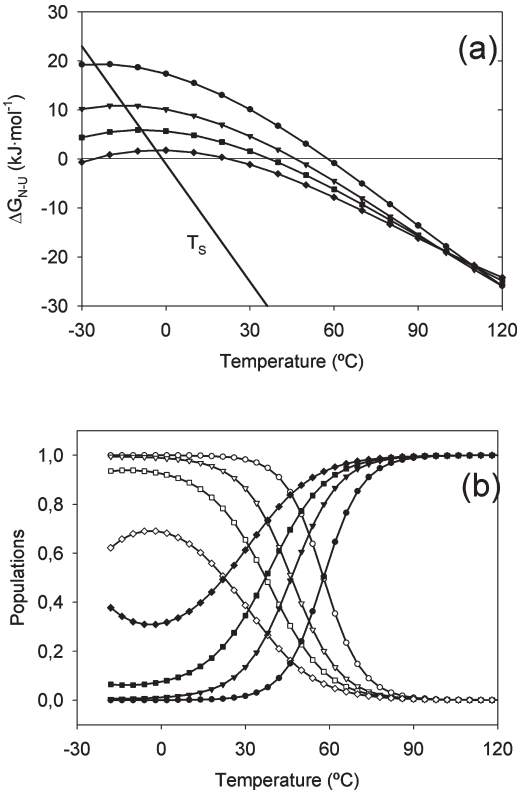

FIGURE 6: Gibbs energy and population analysis of hNedd4-WW4 folding. (a) Gibbs energy changes of unfolding of the hNedd4-WW4 domain found by curve fitting at several pH values. Solid lines with symbols represent stability functions $\Delta G_{N-U}(T)$ as a function of pH, from top to bottom: pH 7 (●), pH 6 (▼), pH 5 (■), and pH 4 (◆). The straight solid line corresponds to the pH dependence of the T_S value. (b) Simulated profiles for the temperature dependence of the populations of unfolded (filled symbols) and folded (empty symbols) states for the hNedd4-WW4 domain under different pH conditions. The parameters of the simulations are listed in Table 1. Symbols for the pH conditions are the same as those described in panel a.

Stability Curves Reveal Marginal Stability and an Anomalously Low T_S Value for the hNedd4-WW4 Domain. We calculated the temperature dependence of the Gibbs energy function at the different pH values and the corresponding populations for the native and denatured states (Figure 6). It appears that hNedd4-WW4 is only marginally stable, the Gibbs energy values being as much as 20 kJ/mol under maximum stability conditions (Table 1). The stability curves obtained under all pH conditions converge at 120 °C (Figure 6a), which is a realistic value according to the statistics mentioned above (*27*). Nevertheless, it is important to note that hNedd4-WW4 is characterized by a strikingly low maximum-stability temperature (T_S), which ranges from −25 °C at pH 7 to −3 °C at pH 4 (Table 1). Even though the information about T_S values for different proteins is scarce, a recent compilation (*23*) clearly shows that even for small proteins (50−60 residues) T_S is well above 0 °C, with values in some cases close to 30 °C. To the best of our knowledge, the lowest value reported to date is that

corresponding to CI2, characterized by a T_S of −8 °C under maximum pH stability conditions (*32*), which is still significantly higher than the value of −25 °C obtained for our system.

At this point, a question concerning the significance of such a low T_S in this protein system arises. It is interesting to remember that increasing the T_S parameter is a well-described evolutionary strategy through which some thermophilic proteins achieve their stability at high temperatures, by a significant rigidification of their native states (*33*−*35*). Thus, the anomalously low T_S value characteristic of the hNedd4-WW4 domain, naturally involved in protein−protein interactions, may reflect the need for high plasticity and flexibility in the native state required for the accommodation of relatively large protein ligands in the binding site. This is well illustrated by the fact that the W17F mutant of the hYAP-WW domain, which is seriously destabilized and mostly unfolded in solution, retains the capacity to bind to its peptide partner in a coupled binding−folding process (*4*).

A Higher Than Normal $C_{pN}(293)$ Confirms a High Level of Flexibility in the Native State of hNedd4-WW4. The considerable conformational flexibility of hNedd4-WW4 is also reflected in the magnitude of the native-state absolute heat capacity [$C_{pN}(293) = 1.73 \pm 0.2$ J K^{-1} g^{-1}], which is well above the value of 1.3 ± 0.3 J K^{-1} g^{-1} obtained as an average from different databases of two-state proteins, and traditionally accepted as a universal value for globular proteins (Figure 5) (*36*, *37*). Nevertheless, the hNedd4-WW4 $C_{pN}(293)$ value lies within the interval provided by more recent statistics over a wider set of native globular proteins, with values ranging from 1.25 to 1.8 J K^{-1} g^{-1} (*38*).

Atypical heat capacity behavior of the pretransition baselines has been reported elsewhere for other systems, such as some leucine zipper constructs (*27*, *39*), BBL (*9*), or gpW protein (*10*). Nevertheless, in these cases, in addition to the anomalously high $C_{pN}(293)$ values, strong temperature dependences of the native-state heat capacity were observed. Bearing in mind that it is well-known that pre- and post-transition baselines are closely correlated to enthalpy fluctuations in the corresponding macroscopic states (native and denatured, respectively) (*27*, *29*, *36*, *40*, *41*), these anomalously high values have been interpreted in terms of more complex, non-two-state equilibria. The leucine zipper constructs have been described in terms of multistate equilibria, whereas gpW has been considered to be at the boarderline of downhill folding (*10*). In the case of BBL, these features have been proposed to support a downhill folding mechanism, with the strong temperature dependence of the native heat capacity reflecting the progressive change in the ensemble properties (*9*).

In our case, in spite of the elevated value of the $C_{pN}(T)$ function, its slope is that expected for a protein of this size (Figure 5). This indicates that the dynamic fluctuations within macrostates would have a noncooperative nature, being thus established between iso-enthalpic conformations (*36*, *42*). This suggests, therefore, a barrier-limited scenario for the equilibria between such macroscopic states in the hNedd4-WW4 domain. An alternative explanation for the anomalous experimental $C_{pN}(293)$ value could be the presence of a conformationally different folded state, which would also be consistent with the scattering in T_m values and the absence of an isosbestic point observed for hNedd4-WW4 (*43*, *44*). Thus, the equilibrium between two different N states might give rise to a contribution to the enthalpy changes that will justify the high $C_{pN}(T)$ values (*44*). Let us say that this phenomenon has been well reported in some other examples, one of them being the FBP28-WW domain, where the conformational change at the N state is similarly attained through the switch provoked by a single residue, as a response to the presence of different types of ligands (*6*).

Double-Perturbation Experiments: Can a Downhill Equilibrium Be Ruled Out?. To further investigate the nature of the conformational equilibrium of hNedd4-WW4, we have analyzed the coupling of thermal and chemical denaturation. These double-perturbation experiments have been put forward as a suitable tool for discerning between the different types of equilibria (*11*): in a barrier-limited scenario, the contributions of both the folded and unfolded states would cause a linear coupling of the thermodynamic parameters (*17*, *23*), while in a multistate or downhill barrier-less process, a nonlinear coupling would be expected, reflecting the continuous change of the conformational ensemble (*9*). This one-state mechanism would also be associated with some other features, like the intersection of the phenomenological baselines deriving from the analysis within the experimentally accessible temperature range, which is incompatible with any process involving an energy barrier. With the knowledge that the baselines reflect the structural properties of the ensemble, the N and U states would have the same structural content at the intersection temperature (*11*).

The results of the double-perturbation experiments conducted with hNedd4-WW4 are summarized in Figure 7, where the thermal unfolding profiles at 230 nm corresponding to urea concentrations ranging from 0 to 6 M in 20 mM phosphate buffer (pH 7) are shown (Figure 7a). The most salient feature of this set of thermal profiles is the progressive downshift of the native CD signals at low temperatures concomitant with an increase in urea concentration. This, in principle, could be indicative of downhill folding (*11*), although it might also be explained by the onset of cold denaturation within the context of a two-state equilibrium.

As can be seen in Figure 7a, the two-state fitting reproduces the effects at low temperatures by interpreting them as cold denaturation. Moreover, parallel baselines were obtained from this analysis, showing similar temperature dependences and thus not intersecting within the experimental temperature range (*9*, *11*, *14*, *17*, *21*, *23*, *24*). The T_m and ΔH_m values show a very good linear correlation [$r = 0.995$ (data not shown)] with urea concentration, and the heat capacity change is comparable to that obtained from thermal denaturation. In addition, it has been proposed that a curvature on the dependency of the unfolding enthalpy at 25 °C with denaturant concentration might indicate a downhill folding (*9*, *10*). No major deviations from the linear behavior are observed for hNedd4-WW4 (Figure 7b).

To definitely distinguish among the two possible folding scenarios in hNedd4-WW4, it would be desirable to obtain experimental evidence for the cold denaturation predicted by the two-state analysis of CD data (Figure 7a). To this end, we have undertaken several DSC experiments at different urea concentrations (Figure 7c) that did not provide clear evidence of a cold denaturation transition. Nonetheless, a shift in $C_{pN}(T)$ toward higher values concomitantly with increasing urea concentration (from 9−10 kJ K^{-1} mol^{-1} in the absence of urea to 20 kJ K^{-1} mol^{-1} at 4.8 M urea) is observed, which parallels the shift in the native signal found for the CD unfolding profiles (Figure 7). Even though this behavior may be interpreted as evidence of downhill folding, it could also be correlated with the increase in heat capacities associated with cold denaturation, bearing in mind that the linear heat capacity measured experimentally might result from the overlapping of two wide and flat

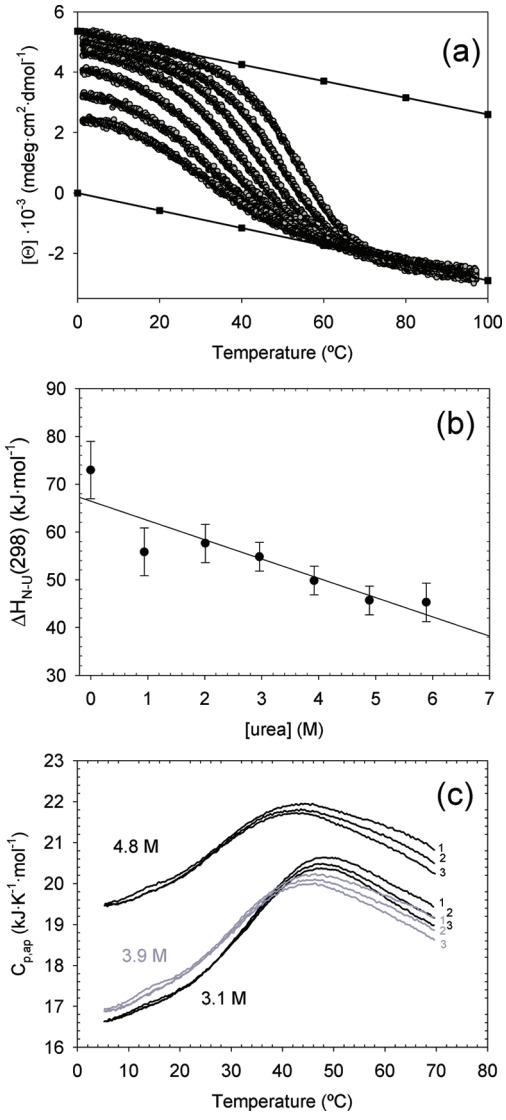

FIGURE 7: Urea dependence of thermal denaturation followed by CD at 230 nm (θ_{230}) for the hNedd4-WW4 domain in 20 mM phosphate (pH 7). (a) Empty circles show the experimental data at 0, 0.94, 2.01, 2.96, 3.92, 4.89, and 5.98 M urea (from right to left), and the baselines $\theta_{230,N}(T)$ (above) and $\theta_{230,U}(T)$ (below), as determined by the multiple-curve fittings, are represented by solid black lines accompanied by squares. The solid lines show the results of the multiple-curve fitting to the two-state model, as described in the text (see Experimental Procedures for details), using the optimized value for $\Delta C_{pN\text{-}U}$ of 2.6 kJ K^{-1} mol^{-1} determined via the ΔH_m vs T_m analysis. (b) Unfolding enthalpy values extrapolated at 298 K, plotted vs urea concentration. The solid line is the linear regression of data. Error bars have been obtained by propagation of fitting errors. (c) Normalized DSC unfolding traces of the hNedd4-WW4 domain obtained at pH 7 and different mid-urea concentrations. Three sucesive heatings conducted for each sample in the calorimeter cell are shown and numbered accordingly. Protein samples were heated to 70 °C to avoid thermal effects associated with urea degradation phenomena.

unfolding transitions. It is important to note that the simulation of the expected DSC heat capacity profiles for hNedd4-WW4 in the presence of urea yields curves very similar to those obtained experimentally (Figure 7c). Thus, even in a two-state scenario, for small proteins characterized by low cooperativity and wide transitions, it would be difficult to observe experimentally a well-defined increase in heat capacity at low temperatures associated with a cold denaturation transition, as has been described for other highly cooperative proteins (*45*).

In summary, the linear dependence of the unfolding enthalpies with both temperature and urea concentration indicates, in principle, a two-state equilibrium, but the inconclusive cold denaturation experiments and the similarities between our double-perturbation profiles and those described elsewhere for downhill folding proteins (*9*−*11*) argue against this hypothesis. Moreover, although the two-state model describes the experimental behavior reasonably, the thermodynamic parameters obtained for hNedd4-WW4 are somewhat similar to those reported for downhill proteins such as BBL (*9*) and gpW (*10*).

Taken together, our data seem to indicate that hNedd4-WW4 could be at the limit of what might be considered a cooperative two-state equilibrium and reflect the lowering of the energy barrier between the different macro states induced by changes in the experimental conditions, such as the presence of chemical denaturants. The small size of the barrier is also supported by previous studies on WW domains reporting on the possible shift between two different native-state ensembles in FBP28-WW (*6*) and on the induced cooperative folding of the W17F mutant in hYap-WW upon ligand binding (*4*). Within this context, the anomalous T_S and $C_{pN}(293)$ values obtained for hNedd4-WW4 are indicative of the high conformational flexibility of the N state.

Evidence of a defined barrier in WW domains is also provided by the hierarchical folding transition state where the presence of a folding nucleus invariably located at the first β-turn has been shown (*7*, *8*). The picture of a polarized transition state with rate-limiting β-turn formation has been also reported for other all β-sheet two-state proteins like SH3 domains and CspB (*46*). In addition, the folding−unfolding rate constants are a bit slower than those for downhill folders that will approach the folding speed limit (*7*, *8*). Thus, the kinetic studies with WW domains reinforce the idea of a common and barrier-limited folding mechanism for β-structures.

One recent computational study with PIN1-WW has arrived at similar conclusions, suggesting that the domain might exhibit downhill behavior at nonphysiologically low temperatures (*47*). These low-temperature effects parallel those observed with our system upon addition of urea. Thus, the results presented here are in agreement with the hypothesis that two-state and downhill equilibria do not constitute two distinctly separate classes but rather extreme limits of a range of possible behaviors determined by the height of the folding barriers, which could be modulated by experimental conditions. Within this context, naturally occurring proteins appear to exhibit cooperative folding transitions and well-defined macroscopic states under physiologically relevant conditions (*46*). Evolutionary pressure at the sequence level against amyloid formation from stable non-native states may be one important reason for such behavior. In the case of the hNedd4-WW4 domain, the relatively large size of ligands when compared to the whole domain might require sufficient structural and dynamic flexibility on the part of the latter to properly accommodate the former, which might even include the organization of an alternative N state. The thermodynamic characterization of other WW domains and marginally stable proteins can be of special interest for acquiring a deeper understanding of the folding equilibria at the limits of cooperativity.

ACKNOWLEDGMENT

We thank our colleague Dr. Jon Trout for revising our English text.

REFERENCES

1. Daggett, V. (2000) Long timescale simulations. *Curr. Opin. Struct. Biol. 10*, 160–164.
2. Ferguson, N., Johnson, C. M., Macias, M., Oschkinat, H., and Fersht, A. (2001) Ultrafast folding of WW domains without structured aromatic clusters in the denatured state. *Proc. Natl. Acad. Sci. U.S.A. 98*, 13002–13007.
3. Koepf, E. K., Petrassi, H. M., Sudol, M., and Kelly, J. W. (1999) WW: An isolated three-stranded antiparallel β-sheet domain that unfolds and refolds reversibly: Evidence for a structured hydrophobic cluster in urea and GdnHCl and a disordered thermal unfolded state. *Protein Sci. 8*, 841–853.
4. Koepf, E. K., Petrassi, H. M., Ratnaswamy, G., Huff, M. E., Sudol, M., and Kelly, J. W. (1999) Characterization of the structure and function of W → F WW domain variants: Identification of a natively unfolded protein that folds upon ligand binding. *Biochemistry 38*, 14338–14351.
5. Crane, J. C., Koepf, E. K., Kelly, J. W., and Gruebele, M. (2000) Mapping the transition state of the WW domain β-sheet. *J. Mol. Biol. 298*, 283–292.
6. Karanicolas, J., and Brooks, C. L.III (2004) Integrating folding kinetics and protein function: Biphasic kinetics and dual binding specificity in a WW domain. *Proc. Natl. Acad. Sci. U.S.A. 101*, 3432–3437.
7. Petrovich, M., Jonsson, A. L., Ferguson, N., Daggett, V., and Fersht, A. R. (2006) Phi-analysis at the experimental limits: Mechanism of β-hairpin formation. *J. Mol. Biol. 360*, 865–881.
8. Sharpe, T., Jonsson, A. L., Rutherford, T. J., Daggett, V., and Fersht, A. R. (2007) The role of the turn in β-hairpin formation during WW domain folding. *Protein Sci. 16*, 2233–2239.
9. Naganathan, A. N., Perez-Jimenez, R., Sanchez-Ruiz, J. M., and Munoz, V. (2005) Robustness of downhill folding: Guidelines for the analysis of equilibrium folding experiments on small proteins. *Biochemistry 44*, 7435–7449.
10. Fung, A., Li, P., Godoy-Ruiz, R., Sanchez-Ruiz, J. M., and Munoz, V. (2008) Expanding the realm of ultrafast protein folding: gpW, a midsize natural single-domain with $\alpha+\beta$ topology that folds downhill. *J. Am. Chem. Soc. 130*, 7489–7495.
11. Oliva, F. Y., and Munoz, V. (2004) A simple thermodynamic test to discriminate between two-state and downhill folding. *J. Am. Chem. Soc. 126*, 8596–8597.
12. Cobos, E. S., Pisabarro, M. T., Vega, M. C., Lacroix, E., Serrano, L., Ruiz-Sanz, J., and Martinez, J. C. (2004) A miniprotein scaffold used to assemble the polyproline II binding epitope recognized by SH3 domains. *J. Mol. Biol. 342*, 355–365.
13. Gill, S. C., and von Hippel, P. H. (1989) Calculation of protein extinction coefficients from amino acid sequence data. *Anal. Biochem. 182*, 319–326.
14. Viguera, A. R., Martinez, J. C., Filimonov, V. V., Mateo, P. L., and Serrano, L. (1994) Thermodynamic and kinetic analysis of the SH3 domain of spectrin shows a two-state folding transition. *Biochemistry 33*, 2142–2150.
15. Privalov, P. L., and Makhatadze, G. I. (1990) Heat capacity of proteins. II. Partial molar heat capacity of the unfolded polypeptide chain of proteins: Protein unfolding effects. *J. Mol. Biol. 213*, 385–391.
16. Zhou, Y. Q., Hall, C. K., and Karplus, M. (1999) The calorimetric criterion for a two-state process revisited. *Protein Sci. 8*, 1064–1074.
17. Cobos, E. S., Filimonov, V. V., Galvez, A., Valdivia, E., Maqueda, M., Martinez, J. C., and Mateo, P. L. (2002) The denaturation of circular enterocin AS-48 by urea and guanidinium hydrochloride. *Biochim. Biophys. Acta 1598*, 98–107.
18. Woody, R. W. (1994) Contributions of tryptophan side chains to the far-ultraviolet circular dichroism of proteins. *Eur. Biophys. J. 23*, 253–262.
19. Sreerama, N., and Woody, R. W. (2003) Structural composition of βI- and βII-proteins. *Protein Sci. 12*, 384–388.
20. Wu, J., Yang, J. T., and Wu, C. S. (1992) β-II conformation of all-β proteins can be distinguished from unordered form by circular dichroism. *Anal. Biochem. 200*, 359–364.
21. Nicholson, E. M., and Scholtz, J. M. (1996) Conformational stability of the *Escherichia coli* HPr protein: Test of the linear extrapolation method and a thermodynamic characterization of cold denaturation. *Biochemistry 35*, 11369–11378.
22. Reid, K. L., Rodriguez, H. M., Hillier, B. J., and Gregoret, L. M. (1998) Stability and folding properties of a model β-sheet protein, *Escherichia coli* CspA. *Protein Sci. 7*, 470–479.
23. Felitsky, D. J., and Record, M. T.Jr. (2003) Thermal and urea-induced unfolding of the marginally stable lac repressor DNA-binding domain: A model system for analysis of solute effects on protein processes. *Biochemistry 42*, 2202–2217.
24. Knapp, S., Mattson, P. T., Christova, P., Berndt, K. D., Karshikoff, A., Vihinen, M., Smith, C. I., and Ladenstein, R. (1998) Thermal unfolding of small proteins with SH3 domain folding pattern. *Proteins 31*, 309–319.
25. Martinez, J. C., el Harrous, M., Filimonov, V. V., Mateo, P. L., and Fersht, A. R. (1994) A calorimetric study of the thermal stability of barnase and its interaction with 3′GMP. *Biochemistry 33*, 3919–3926.
26. Martinez, J. C., Filimonov, V. V., Mateo, P. L., Schreiber, G., and Fersht, A. R. (1995) A calorimetric study of the thermal stability of barstar and its interaction with barnase. *Biochemistry 34*, 5224–5233.
27. Privalov, P. L., and Dragan, A. I. (2007) Microcalorimetry of biological macromolecules. *Biophys. Chem. 126*, 16–24.
28. Candel, A. M., van Nuland, N. A., Martin-Sierra, F. M., Martinez, J. C., and Conejero-Lara, F. (2008) Analysis of the thermodynamics of binding of an SH3 domain to proline-rich peptides using a chimeric fusion protein. *J. Mol. Biol. 377*, 117–135.
29. Robertson, A. D., and Murphy, K. P. (1997) Protein Structure and the Energetics of Protein Stability. *Chem. Rev. 97*, 1251–1268.
30. Fu, L., and Freire, E. (1992) On the origin of the enthalpy and entropy convergence temperatures in protein folding. *Proc. Natl. Acad. Sci. U.S.A. 89*, 9335–9338.
31. Hilser, V. J., Gomez, J., and Freire, E. (1996) The enthalpy change in protein folding and binding: Refinement of parameters for structure-based calculations. *Proteins 26*, 123–133.
32. Jackson, S. E., and Fersht, A. R. (1991) Folding of chymotrypsin inhibitor 2. 1. Evidence for a two-state transition. *Biochemistry 30*, 10428–10435.
33. Razvi, A., and Scholtz, J. M. (2006) Lessons in stability from thermophilic proteins. *Protein Sci. 15*, 1569–1578.
34. Nojima, H., Ikai, A., Oshima, T., and Noda, H. (1977) Reversible thermal unfolding of thermostable phosphoglycerate kinase. Thermostability associated with mean zero enthalpy change. *J. Mol. Biol. 116*, 429–442.
35. Jaenicke, R. (2000) Do ultrastable proteins from hyperthermophiles have high or low conformational rigidity? *Proc. Natl. Acad. Sci. U.S.A. 97*, 2962–2964.
36. Privalov, P. L., and Khechinashvili, N. N. (1974) A thermodynamic approach to the problem of stabilization of globular protein structure: A calorimetric study. *J. Mol. Biol. 86*, 665–684.
37. Freire, E. (1995) in Protein stability and folding: Theory and practice (Shirley, B. A., Ed.) pp 191−218, Humana Press Inc., Totowa, NJ.
38. Makhatadze, G. I. (1998) Heat capacities of amino acids, peptides and proteins. *Biophys. Chem. 71*, 133–156.
39. Dragan, A. I., and Privalov, P. L. (2002) Unfolding of a leucine zipper is not a simple two-state transition. *J. Mol. Biol. 321*, 891–908.
40. Freire, E., Hayne, D. T., and Xie, D. (1993) Molecular basis of cooperativity in protein folding. 4. Core: A general cooperative folding model. *Proteins: Struct., Funct., Genet. 17*, 111–123.
41. Makhatadze, G. I., and Privalov, P. L. (1995) Energetics of protein structure. *Adv. Protein Chem. 47*, 307–425.
42. Cooper, A. (1976) Thermodynamic fluctuations in protein molecules. *Proc. Natl. Acad. Sci. U.S.A. 73*, 2740–2741.
43. Arbely, E., Rutherford, T. J., Sharpe, T. D., Ferguson, N., and Fersht, A. R. (2009) Downhill versus barrier-limited folding of BBL 1: Energetic and structural perturbation effects upon protonation of a histidine of unusually low pKa. *J. Mol. Biol. 387*, 986–992.
44. Settanni, G., and Fersht, A. R. (2009) Downhill versus barrier-limited folding of BBL 3. Heterogeneity of the native state of the BBL peripheral subunit binding domain and its implications for folding mechanisms. *J. Mol. Biol. 387*, 993–1001.
45. Privalov, P. L. (1990) Cold denaturation of proteins. *Crit. Rev. Biochem. Mol. Biol. 25*, 281–305.
46. Royer, C. A. (2008) The nature of the transition state ensemble and the mechanisms of protein folding: A review. *Arch. Biochem. Biophys. 469*, 34–45.
47. Bruscolini, P., Pelizzola, A., and Zamparo, M. (2007) Downhill versus two-state protein folding in a statistical mechanical model. *J. Chem. Phys. 126*, 215103.